Nano Energy 49 (2018) 1–6

Contents lists available at ScienceDirect

Nano Energy

journal homepage: www.elsevier.com/locate/nanoen

Communication

Probing electrical degradation of cathode materials for lithium-ion batteries with nanoscale resolution

Seong Yong Park[a], Woon Joong Baek[a], Seung Yeon Lee[a], Jin Ah Seo[b], Yoon-Sok Kang[b], Meiten Koh[b], Seong Heon Kim[a,*]

[a] Analytical Engineering Group, Samsung Advanced Institute of Technology, 130 Samsung-ro, Yeongtong-gu, Suwon-si, Gyeonggi-do 443-803, Republic of Korea
[b] Energy Laboratory, Samsung Advanced Institute of Technology, 130 Samsung-ro, Yeongtong-gu, Suwon-si, Gyeonggi-do 443-803, Republic of Korea

ARTICLE INFO

Keywords:
Lithium-ion battery
$LiNi_xCo_yAl_zO_2$
Microcrack
SSRM

ABSTRACT

Understanding the degradation mechanism of Lithium-ion batteries (LIBs) is critical in developing high-performance LIBs, and the investigation of their electrical conductivity evolution during cycling can lead to a better understanding of the degradation mechanism of the cathode materials for Li-ion batteries (LIBs). Here, we studied the evolution of the electrical conductivity of $LiNi_{0.8}Co_{0.15}Al_{0.05}O_2$ (NCA) particles for LIB cathodes using scanning spreading resistance microscopy (SSRM). After 300 charge/discharge cycles, stepwise-increasing resistance distributions toward the centers of the secondary particles are observed. These distributions correspond to the degenerated granular structures of the secondary particles caused by the formation of microcracks. In addition, the correlation between the electrical conductivity and microstructure of the NCA cathode is established to explain the observed decay of the NCA discharge capacity. Our findings can provide an insight into the debatable degradation mechanism of LIB cathode materials such as NCA and NMC ($LiNi_xMn_yCo_zO_2$, $x + y + z = 1$).

1. Introduction

Lithium-ion batteries (LIBs) are considered to be one of the most important battery technologies, since they are widely utilized in personal electronic devices such as smartphones, laptop computers, digital cameras, and health monitoring systems. In addition, they are used in modern electric vehicles (EVs) owing to their superior energy density [1–4]. However, various parameters of the current LIB models (including cycle life, charging speed, and safety during operation) must be significantly improved for their successful application in EVs. Among several candidate materials for large-size applications (e.g., electric vehicles), Ni-based layered materials such as $LiNi_{.8}Co_{.15}Al_{.05}O_2$ (NCA) and $LiNi_xCo_yMn_zO_2$ ($x + y + z = 1$) are more promising than those made of $LiCoO_2$ (which are mainly used in small electronic devices), owing to their high energy density and low production costs.

Multiple research studies have been conducted to elucidate the possible reasons for the observed decay of the discharge capacity of Ni-based layered cathode materials on the microscopic and macroscopic scales using X-ray techniques, scanning electron microscopy (SEM), transmission electron microscopy (TEM), and various spectroscopic methods [5–12]. The possible reasons for the cathode degradation during cycling include phase transitions from the original $R\bar{3}m$ layered structure to spinel or rock salts, the development of microcracks, porosity formation, irreversible movements of Li ions, losses of oxygen species, and metal dissolution [8–11,13,14]. However, direct correlations between these phenomena and the deteriorated electrical performance of the cathode have not yet been established. Researchers have found that the application of conductive coatings and the reduction in particle size significantly enhanced the cathode conductivity and thus improved the overall battery performance [15–18]. Therefore, the investigation of the electrical conductivity evolution during cycling can lead to a better understanding of the degradation mechanism of cathode materials.

Scanning spreading resistance microscopy (SSRM) is a technique based on atomic force microscopy (AFM), which is often utilized for studying two-dimensional (2D) electrical conductivity and the resistance of various materials with nanometer spatial resolutions (Fig. 1a). When a conductive probe scans the sample surface in the contact mode, the resulting electrical spreading resistance is recorded; thus, this technique is widely utilized for studying 2D carrier or dopant distributions in semiconductor devices [19]. In this work, we adopted the SSRM as a main tool to examine the electrical properties of NCA cathode materials by visualizing the electrical conductivity of NCA particles during cycling. The obtained resistance distributions were

* Corresponding author.
E-mail address: sh712.kim@samsung.com (S.H. Kim).

https://doi.org/10.1016/j.nanoen.2018.04.005
Received 1 February 2018; Received in revised form 22 March 2018; Accepted 3 April 2018
Available online 04 April 2018

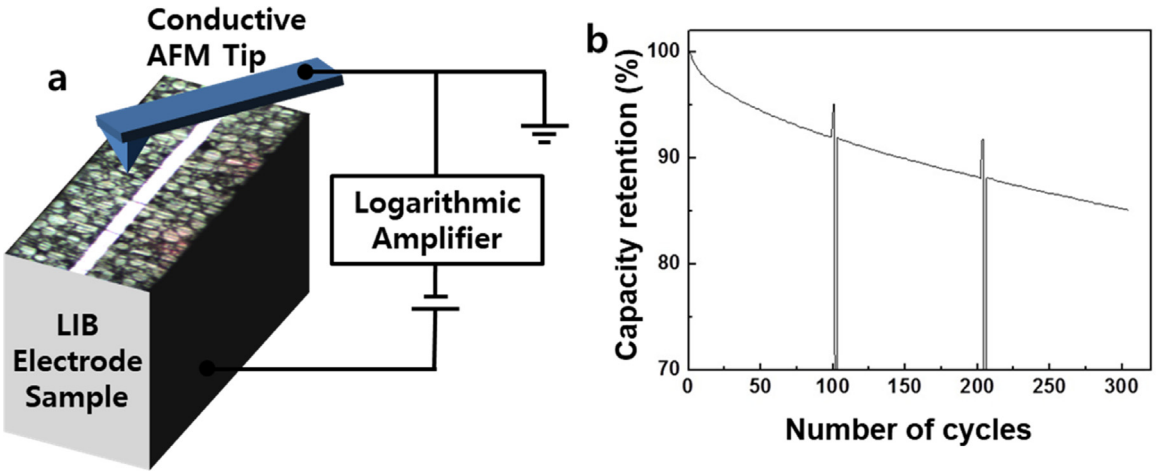

Fig. 1. (a) Schematic of SSRM on the cross-sectional NCA cathode sample. (b) Capacity retention of the full NCA/graphite cell during the first 300 charge/discharge cycles.

analyzed by considering the physical microstructure investigated via electron microscopy, and the relationship between these two parameters was used to explain the observed decay of the cathode discharge capacity.

Cylindrical 18650-type Li-ion cells with NCA cathodes and graphitic anodes were fabricated in this study. The cathodes were composed of NCA (secondary) particles, Denka black, and polyvinylidene fluoride, while the anodes were produced from graphite, styrene-butadiene rubber, and carboxymethyl cellulose. NCA secondary particles had a bimodal size distribution with ~11 μm (large) and ~3 μm (small), which were agglomerated with primary particle of ~1 μm size. The electrolyte solution was prepared by mixing fluoroethylene carbonate, ethylene carbonate, ethyl methyl carbonate, dimethyl carbonate (DMC), and vinylene carbonate with 1.15 M of $LiPF_6$. The fabricated cells were charged and discharged at a constant rate of 1 C and a temperature of 45 °C for 4.3 V and 2.8 V, respectively. A total of 300 charge/discharge cycles were performed after 3 formation cycles. The fully discharged cells were disassembled, and their electrodes were washed with DMC and dried overnight in a glove box filled with Ar. The sample preparation was conducted inside the glove box, which was connected to the utilized analytical equipment via a vacuum transfer system to minimize the additional degradation of the studied Li-based electrodes caused by the presence of oxygen and moisture in the air. To perform microscopic observations and resistance measurements of the pristine and cycled NCA electrodes, their cross-sectional specimens were prepared under cryogenic conditions at a temperature of − 140 °C using the Ar ion beam with an energy of 5 keV. SEM, conductive atomic force microscopy (C-AFM), and SSRM measurements were conducted on the fabricated cross-sectional samples. TEM observations were performed using the specimens prepared by a focused ion beam lift-out technique.

The discharge capacity of the studied cells was decreased by about 85% after 300 charge/discharge cycles from 476 mAh to 402 mAh (Fig. 1b; the cross-sectional microstructure of the cathode is depicted in Fig. 2a). For the nanoscale mapping of the electrical properties, the conductive AFM probe tip was in contact with the surface of the cross-sectional NCA cathode sample, which was previously polished by Ar ions. As shown in Fig. 1a, with applying the appropriate bias voltage (3 V in this study), the current passing through the sample between the tip and the sample base (Al current collector) are measured using a logarithmic current amplifier in SSRM, while a linear current amplifier is used in conventional C-AFM. In most cases, the measured current value can be converted to a resistance one in SSRM. By scanning the sample surface and repeating the resistance (current) measurements, 2D topographic and resistance (current) images are acquired simultaneously. In particular, the usage of logarithmic current amplifier widens the range of resistance (typically 10^4–10^{11} Ω) which can be measured and a wide range of samples, from insulating through semiconducting to metallic, can be studied in SSRM. Because SSRM is operated in contact AFM mode and requires a stable electrical contact, conductive diamond-coated tips (CDT-NCHR, NanoWorld) were used in this study, which have the typical tip radius of curvature ranged between 100 and 200 nm.

The results of the C-AFM analysis revealed no significant differences between the pristine and cycled samples; only the highly conductive matrix was detected because of the presence of conductive additives and less conductive NCA secondary particles, as shown in Fig. 2b and c, respectively. In contrast to the C-AFM studies, the SSRM measurements showed distinct differences between the pristine and cycled samples because SSRM could be operated in a wider range of resistance (typically 10^4 -10^{11} Ω). As shown in Figs. 2e and 3b, the secondary NCA particles in pristine cathodes were characterized by uniform resistance, which was approximately one order of magnitude higher than that of the conductive agent region of dark blue color. (The yellow region in Figs. 2e and 3b may indicate the intrinsically non-conductive binder or the electrically isolated conductive agent materials.) However, in Figs. 2g and 3d, the secondary particles in the cycled samples exhibited a resistance distribution that was different from that obtained for the pristine NCA. It should be noted that the primary particles showed various resistances that changed in a stepwise manner within the secondary particles. As shown in the line profiles of resistance (Fig. 3e), the observed variation in resistance within the cycled secondary particle was as high as four orders of magnitude. The variation in resistance distribution within the cycled secondary particle was confirmed by comparing the statistical plots of the resistance values (Fig. 3f). In Fig. 3f, while the resistance values acquired on the central area of pristine particle were distributed from ~10^5 to ~10^7 Ω, those of the cycled particle spread from ~10^5 to ~10^{10} Ω. The substantial change in the electrical resistance of the primary particles indicated that the movement of electrons and Li ions from/to this region was inhibited. As a result, the primary particles of high resistance became less active than the particles of low resistance under the same charge/discharge operation conditions, thus decreasing the cathode discharge capacity.

Fig. 4 shows another SSRM result acquired from a different 300-cycled sample. In the resistance image (Fig. 4b), the overall degradation trend is almost the same as that shown in Figs. 2g and 3d. However, the secondary particle indicated by the black arrow in Fig. 4b shows a different resistance characteristic than other neighboring particles. The indicated particle shows increased resistance on the entire area. It may be possible that the degradation process for this specific particle was